Photothermally Enhanced Drug Delivery by Ultrasmall Multifunctional FeCo/Graphitic Shell Nanocrystals

Sarah P. Sherlock, Scott M. Tabakman, Liming Xie, and Hongjie Dai*

Department of Chemistry, Stanford University, Stanford, California 94305, United States

ABSTRACT FeCo/graphitic carbon shell (FeCo/GC) nanocrystals (~4−5 nm in diameter) with ultrahigh magnetization are synthesized, functionalized, and developed into multifunctional biocompatible materials. We demonstrate the ability of this material to serve as an integrated system for combined drug delivery, near-infrared (NIR) photothermal therapy, and magnetic resonance imaging (MRI) *in vitro*. We show highly efficient loading of doxorubicin (DOX) by π-stacking on the graphitic shell to afford FeCo/GC−DOX complexes and pH sensitive DOX release from the particles. We observe enhanced intracellular drug delivery by FeCo/GC−DOX under 20 min of NIR laser (808 nm) induced hyperthermia to 43 °C, resulting in a significant increase of FeCo/GC−DOX toxicity toward breast cancer cells. The synergistic cancer cell killing by FeCo/GC−DOX drug delivery under photothermal heating is due to a ~two-fold enhancement of cancer cell uptake of FeCo/GC−DOX complex and the increased DOX toxicity under the 43 °C hyperthermic condition. The combination of synergistic NIR photothermally enhanced drug delivery and MRI with the FeCo/GC nanocrystals could lead to a powerful multimodal system for biomedical detection and therapy.

KEYWORDS: drug delivery · photothermal · MRI · supramolecular chemistry · doxorubicin · multifunctional nanoparticle

The use of nanomaterials in medicine has offered the capability of combining multiple functionalities into a single system. Materials such as inorganic nanoparticles, carbon nanotubes, dendrimers, and liposomes, have all been investigated to combine multiple therapeutic approaches, such as imaging, drug delivery, and photothermal therapy.[1−11] Of particular interest with this class of materials is the ability to gain control over the toxicity of the therapy through controlled release or enhanced therapeutic efficacy.

One means of enhancing therapeutic efficacy has been through combining chemotherapy drugs with hyperthermia. Previous studies have heated regions of the body to target temperatures up to ~43 °C to enhance efficacy of drugs, such as doxorubicin (DOX), an anthracycline antibiotic used to treat a wide variety of cancers.[3,12−18] A drawback of clinical hyperthermia methods, such as limb perfusion, radiowave irradiation, or incubation chambers, is that nonspecific heating can result in enhanced drug effects throughout the general anatomical region, resulting in undesired side effects to normal organs and tissues.[12,13] In an effort to improve the safety of thermal cancer therapies, near-infrared (NIR) absorbing photothermal agents have been explored in combination with laser irradiation to provide site-specific heating and treatment of diseased regions with a high uptake of the photothermal agents.[3,4,15−17]

There has been a recent interest in developing cooperative nanoscale systems to enhance DOX toxicity *via* NIR irradiation.[3,4,15−17] Synergy between DOX and NIR irradiation has been demonstrated through the addition of NIR photothermal agents, such as indocyanine green or gold nanomaterials, to cells subjected to DOX or DOX liposome treatment.[14−16] In these systems, the drug and photothermal sensitizer, or heat inducing material, are separate agents. Systems capable of both drug delivery and photothermal therapy have been developed by creating gold half-shells around DOX-loaded polymer spheres.[3,4,17] While these approaches have shown favorable results, these particles tend to be large (>70 nm) in size and lack the ability to monitor the particle biodistribution *via* a clinically relevant imaging modality. Addition of a magnetic layer under the gold half-shell has imparted MRI capabilities, however, the size of the particles is undesirably large (~100 nm), and therapeutic efficacy has yet to be determined.[17]

In this work, we create a highly integrated nanoparticle system uniquely capable of drug delivery, imaging, and photothermal therapy. To achieve this, we use an ultrasmall ~4 nm magnetic nanocrystal containing a single crystalline iron−cobalt core surrounded by a single- or few-layer graphitic shell (FeCo/GC).[19] The graphitic carbon shell is capable of loading DOX *via* π-stacking and exhibits a

* Address correspondence to hdai@stanford.edu.

Received for review December 10, 2010 and accepted January 24, 2011.

Published online February 01, 2011
10.1021/nn103415x

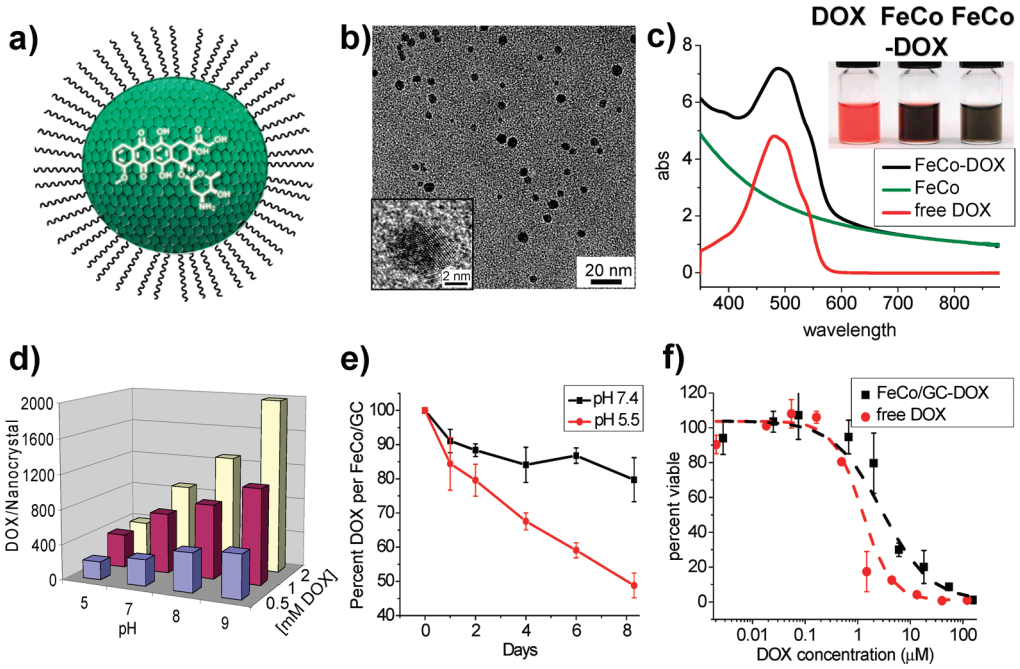

Figure 1. Structure of FeCo/GC−DOX, drug loading and release. (a) Schematic of DOX π-stacking on FeCo/GC. The FeCo core (shown in green) is surrounded by a single layer of graphite. The nanocrystal is made water soluble by a noncovalent interaction with phospholipid-branched PEG. DOX, shown in white, loads noncovalently on the graphitic surface of FeCo/GC. (b) TEM images of FeCo/GC−DOX conjugates. The average diameter is ~4 nm for the FeCo/GC−DOX complex. A high-resolution TEM image of a single FeCo/GC−DOX nanocrystal is shown as the inset. (c) UV−vis absorbance spectra of free DOX, FeCo/GC−DOX (FeCo−DOX), or FeCo/GC (FeCo). The DOX concentration is 450 μM for free DOX and FeCo/GC−DOX samples. The FeCo/GC concentration is ~270 nM for both the FeCo/GC and FeCo/GC−DOX samples. Both free DOX and FeCo/GC−DOX show a characteristic peak around 490 nm. Suspensions of DOX, FeCo/GC−DOX, and FeCo/GC are shown in the inset. (d) Loading of DOX on FeCo/GC shows a strong dependence on pH and DOX concentration during the incubation. The *z*-axis is the number of DOX molecules loaded on a single FeCo/GC nanocrystal (see Methods Section). (e) The release of DOX from the surface of FeCo/GC is accelerated at lower pH. (f) Concentration-dependent cell survival curves of MCF-7 cells incubated with free DOX or FeCo/GC−DOX for 2 days. IC_{50} values of 1.2 and 2.9 μM were calculated for free DOX and FeCo/GC−DOX, respectively.

useful absorbance of NIR light affording photothermal effects. The highly magnetic metal core makes FeCo/GC an advanced MRI contrast agent, as FeCo is known to have one of the highest saturation magnetizations among all materials.[19,20] Therefore, we are developing ultrasmall nanocrystals into a highly multifunctional agent, capable of both drug delivery and photothermal therapy with the additional benefit of tracking the nanoparticle system with a clinically relevant imaging modality.

We show environmentally sensitive loading and release of DOX from the FeCo/GC system, demonstrating faster drug release in acidic conditions that mimic the extracellular tumor environment. The highly controllable loading and release of DOX are attributed to the supramolecular loading of DOX on the graphitic shell of FeCo/GC.[21,22] When used to deliver DOX to MCF-7 cells, a human breast cancer line, FeCo/GC−DOX is slightly less toxic than free DOX, however, when combined with 20 min of NIR photothermal heating to 43 °C a drastic increase in toxicity is observed for cancer cells treated with FeCo/GC−DOX. Using MRI, fluorescence measurements and flow cytometry, we reveal a ~two-fold increase in cellular uptake of FeCo/GC−DOX when incubated for 20 min at 43 °C over 37 °C. The significant increase in cellular uptake of FeCo/GC−DOX under photothermal laser irradiation combined with an increase in DOX efficacy at elevated temperatures could make FeCo/GC−DOX a powerful system for photothermally enhanced drug delivery and MRI-guided cancer therapy.

RESULTS AND DISCUSSION

To obtain highly biocompatible and water-soluble FeCo/GC, nanocrystals synthesized by a chemical vapor deposition method[19] were sonicated with a phospholipid-branched-polyethylene glycol carboxylate (PL-brPEG) and centrifuged to removed aggregates (see Methods Section).[20] The nanocrystals, as depicted in Figure 1a, were well dispersed and stable in buffer solutions and serum,[19] with an average diameter of ~4 nm revealed by transmission electron microscopy TEM (Figure 1b). The nanocrystals are known to have superior chemical stability in acid and air and show no evidence of oxidation or degradation over a monitoring period of 1 month.[19] While the shell does show some disordered nature, as evidenced by both a Raman G and D band, the stability of the nanocrystal in acid demonstrates the nonporous nature of the carbon shell.[19] DOX was loaded noncovalently onto water-soluble FeCo/GC by

simply mixing solutions under controlled pH and DOX concentrations for ~14 h. After removal of free DOX by centrifuge filtration, evidence of DOX loading on FeCo/GC was visible by eye (Figure 1c inset) due to the deep red appearance of the FeCo/GC−DOX suspension. DOX content was quantified using UV−vis absorbance, with a prominent DOX peak appearing around 490 nm over the FeCo/GC background (Figure 1c). Solutions of FeCo/GC−DOX were stable in water and PBS buffer solutions over multiple weeks without significant aggregation.

The degree of loading of DOX onto FeCo/GC showed a strong dependence on both pH and DOX concentration during the DOX loading incubation. By altering the loading conditions, we were able to load between ~200 and ~2000 DOX molecules onto each FeCo/GC nanocrystal (see Methods Section), as shown in Figure 1d. The highest DOX loadings were achieved at basic conditions where the daunosamine group of DOX was deprotonated and the solubility in water reduced. Conversely, at lower pH conditions, DOX solubility was increased, and loading on FeCo/GC is minimized. This suggested hydrophobic interactions and π-stacking as the driving force for DOX loading on FeCo/GC. The aromatic character of DOX enabled π-stacking onto the graphitic sidewall of FeCo/GC in a similar manner to DOX loading on carbon nanotubes and graphene.[21−23] The π-stacking interaction was confirmed by fluorescence quenching of DOX when loaded onto FeCo/GC (see Figure S1, Supporting Information).

The release of DOX from the FeCo/GC surface was a slow, continuous process over the course of multiple days (Figure 1e). This release was accelerated at acidic conditions as the daunosamine group of DOX was protonated and water solubility increased.[24] Samples of FeCo/GC−DOX conjugates dialyzed over 8 days showed that the release of DOX from FeCo/GC is ~three times greater at pH 5.5 than pH 7.4. This activated release in acidic conditions makes our material appealing for drug delivery applications as both the extracellular environment of tumors and the intracellular lysosomes and endosomes are acidic.

The 4 nm nanocrystals showed a slower DOX release profile than single-walled carbon nanotubes (~1 nm diameter), possibly due to a stronger interaction between the DOX and the graphitic sidewall of FeCo/GC.[21] The larger diameter of FeCo/GC has less curvature and may provide a more planar surface for DOX loading, leading to higher drug loading and slower release. The diameter-dependent release was a driving force to use 4 nm nanocrystals over the 7 nm nanocrystals used in previous works.[19,20]

Initial tests on the toxicity of FeCo/GC−DOX conjugates were performed on the human breast adenocarcinoma cell line MCF-7. FeCo/GC−DOX and free DOX were incubated with cells for 2 days prior to viability measurement. Both FeCo/GC−DOX and free DOX induced significant cell death above 10 μM, with less than 20% viable cells after 2 days (Figure 1f). At lower concentrations, free DOX proved to be slightly more toxic than FeCo/GC-bound DOX with IC_{50} values of 1.2 μM (0.7 μg DOX/mL) and 2.9 μM (1.7 μg DOX/mL), respectively (Figure 1f). The decreased toxicity of FeCo/GC−DOX could be attributed to the slow, continual release of DOX from the FeCo/GC surface over the 2 day incubation period. This resulted in lower concentrations of released DOX available for cell killing during the incubation period. It should be noted that the toxicity was only due to DOX as FeCo/GC without drug attached showed no significant toxicity to MCF-7 cells (see Figure S2, Supporting Information).

Graphitic materials, such as carbon nanotubes,[25,10] graphite-oxide,[26] and larger diameter FeCo/GC,[19] have all been shown to generate heat under NIR irradiation. The optical absorbance of the graphitic shell of FeCo/GC−DOX conjugates at ~800 nm makes them an ideal candidate for use with biological systems due to the minimal absorbance of cellular and tissue components at this wavelength.[27] The heating capabilities of FeCo/GC, FeCo/GC−DOX, and DOX were investigated during 808 nm laser irradiation. When samples of 450 μM DOX (260 μg DOX/mL) and FeCo/GC suspensions with or without 450 μM loaded DOX were irradiated with an 808 nm laser at 0.3 W/cm^2, the FeCo/GC-containing samples showed selective graphitic carbon shell-mediated heating over the free DOX solution (Figure 2a and b). Thermal imaging with an infrared camera confirmed a temperature increase of ~35 °C for solutions containing FeCo/GC during the 10 min of laser irradiation (Figure 2c). The ability for efficient photothermal heating of the FeCo/GC−DOX system compared to a free drug suggested the multifunctional therapeutic potential of this ultrasmall, highly integrated system for combined MRI, drug delivery, and NIR photothermal therapy.

To test the photothermal effect of FeCo/GC−DOX in drug delivery, we compared 808 nm laser-irradiated *vs* nonirradiated MCF-7 cells mixed with either FeCo/GC−DOX, free DOX, FeCo/GC, or a PBS control. For the laser irradiated samples, a target temperature of 43 °C for FeCo/GC and FeCo/GC−DOX samples was maintained for 20 min. Cells incubated with either DOX or PBS were irradiated concurrently, although no significant heating was observed. After the 20 min irradiation/incubation period, cells were washed to fully remove the drug and allowed to proliferate for 2 days before viability assessment.

Cell viability measurements demonstrated a significant increase in toxicity for FeCo/GC−DOX when combined with 808 nm photothermal treatment (Figure 3a and b). For nonirradiated MCF-7 cells, FeCo/GC−DOX inhibited cell growth by 27−28% at concentrations of 30 or 60 μg DOX/mL, respectively (Figure 3a). Inclusion of laser irradiation for 20 min afforded a photothermal

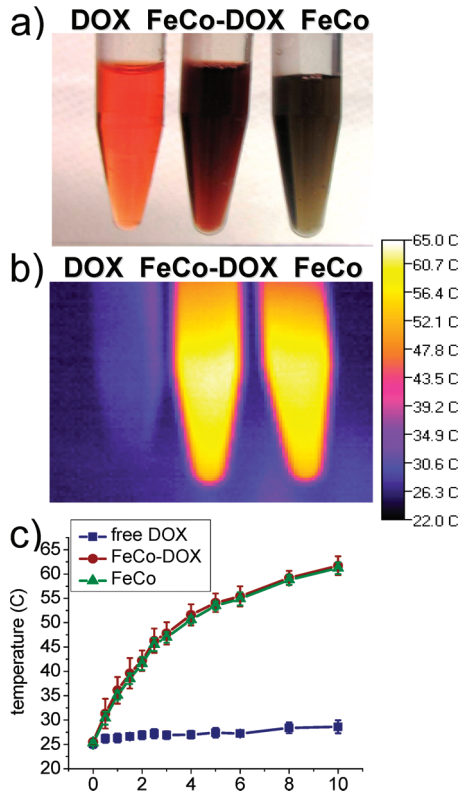

Figure 2. Photothermal heating of DOX and FeCo/GC suspensions. (a) Image of solutions containing 450 μM DOX as either free DOX or FeCo/GC−DOX (FeCo−DOX). The FeCo/GC (FeCo) solution shown has the same FeCo/GC content as the FeCo/GC−DOX solution. (b) Thermal image after 10 min of 808 nm laser irradiation at 0.3 W/cm^2. Both the FeCo/GC−DOX and FeCo/GC samples show significant photothermal heating, while the free DOX solution is not heated by the laser. (c) Temperature measurements from thermal images acquired during the 10 min laser irradiation show a temperature increase of ~35 °C for FeCo/GC containing samples. The free DOX sample showed almost no heating effect from laser irradiation.

heating of the solution to 43 °C during the FeCo/GC−DOX incubation period, resulting in cell growth inhibition of 64 and 69% for the 30 and 60 μg DOX/mL cases respectively (Figure 3a and b). The viability of all other treatment groups (free DOX, FeCo/GC or PBS treated cells) remained similar to their nonirradiated controls (Figure 3a). Addition of photothermal therapy more than doubled the toxicity of FeCo/GC−DOX, causing more cell death than DOX in its free form with or without 808 nm laser irradiation. Importantly, there was no significant reduction in viability for cells incubated with FeCo/GC with or without photothermal heating to 43 °C. This indicated that the FeCo/GC nanocrystals were nontoxic and that photothermal heating of cells to 43 °C for 20 min alone was not sufficient to induce cell death. Additionally, cell viability was not affected in samples subjected to laser irradiation in the absence of a photothermal agent, such as in the PBS and free DOX incubated samples. The target temperature of 43 °C was chosen to enhance DOX toxicity and minimize damage to cells not exposed to the drug.

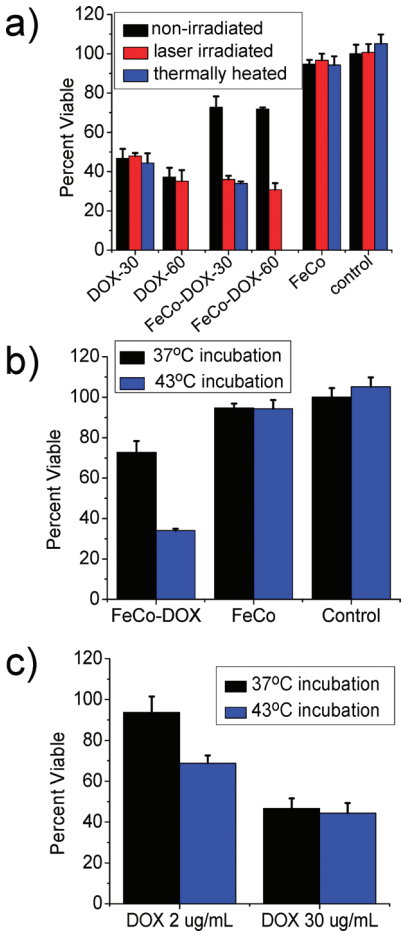

Figure 3. Cellular toxicity enhancement of DOX conjugates when combined with photothermal heating to 43 °C. (a) Cell viability of MCF-7 cells after incubation with free DOX, FeCo/GC−DOX (FeCo−DOX), and FeCo/GC (FeCo). DOX concentrations were either 30 or 60 μg DOX/mL. Samples were incubated for 20 min and combined with heating to 43 °C through photothermal laser heating (red bars) or thermal heating in a water bath (blue bars). Nonheated samples are shown in black. FeCo/GC, free DOX, or untreated control cells showed no viability dependence on the incubation conditions (heated *vs* nonheated). FeCo/GC−DOX efficacy was significantly enhanced when incubations were performed at 43 °C. The viability of control cells or FeCo/GC (FeCo) incubated cells was not affected by laser irradiation or thermal heating to 43 °C for 20 min. (b) MCF-7 viability plots demonstrate the large increase in toxicity resulting from FeCo/GC−DOX (FeCo−DOX) at 43 °C over 37 °C, while cells incubated with FeCo/GC (FeCo) are not affected by thermal heating to 43 °C for 20 min. (c) Cell toxicity of DOX at 37 and 43 °C reveals thermal enhancement of DOX toxicity at low doses of DOX (2 μg/mL). DOX efficacy of highly toxic doses (30 μg/mL) is not enhanced at 43 °C due to the sufficiently high efficacy of high-dose DOX at 37 °C.

To compare with NIR photothermal heating, cells were incubated with FeCo/GC, PBS, FeCo/GC−DOX, or free DOX at 30 μg DOX/mL and heated thermally in a water bath to 43 °C for 20 min. Cells were then washed to remove the drug and allowed to proliferate for 2 days. Cell viability proved to be similar to the laser irradiated case. Compared to cell samples incubated at 37 °C, thermal heating of cells to 43 °C for 20 min afforded much enhanced toxicity resulting from FeCo/GC−DOX

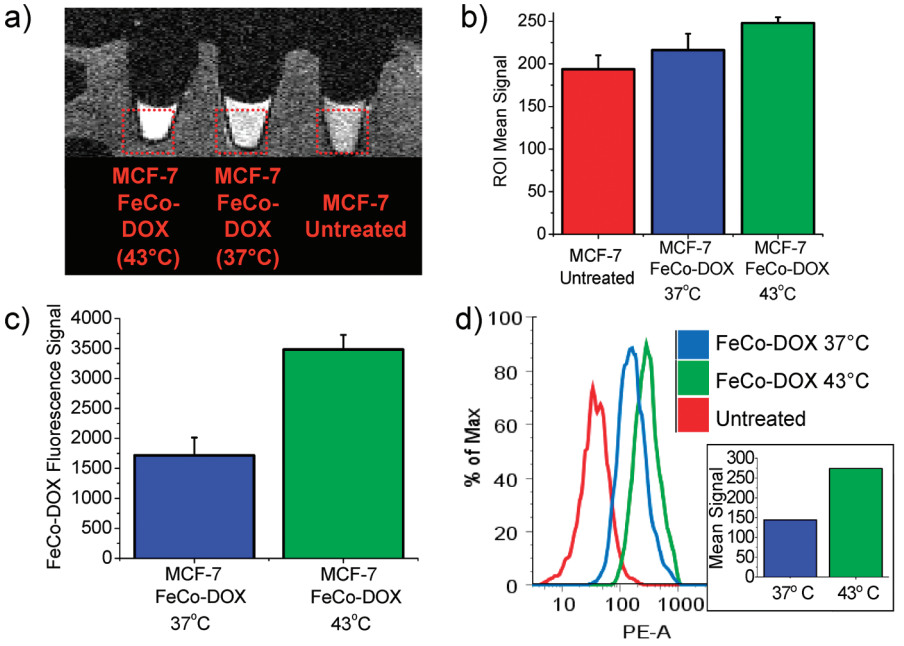

Figure 4. Enhanced cellular uptake of FeCo/GC−DOX at 43 °C. (a) Magnetic resonance image of pelletted, untreated MCF-7 cells or pelletted MCF-7 cells treated with FeCo/GC−DOX (FeCo−DOX) for 20 min at 43 and 37 °C. Brightening of samples in the T_1-weighted images indicates FeCo/GC−DOX uptake. Cells incubated at 43 °C with FeCo/GC−DOX appeared the brightest due to higher cellular uptake of FeCo/GC−DOX. (b) ROI signal measurements of the cell pellets in part (a). MCF-7 cells treated with FeCo/GC−DOX had the highest signal intensity due to the higher uptake during the 20 min incubation. (c) DOX fluorescence signal after being extracted from cells incubated with FeCo/GC−DOX (FeCo−DOX) for 20 min at 37 or 43 °C. (d) Flow cytometry measurements confirming higher DOX fluorescence in cells incubated with FeCo/GC−DOX at 43 °C than at 37 °C. Untreated MCF-7 cell signal is shown for comparison. The mean signal of cells treated with FeCo/GC−DOX for 20 min at 37 °C versus 43 °C is plotted in the inset. The ratio of the 43 °C treatment *vs* the 37 °C treatment is similar to the signal ratio in part (c).

incubation but not for cells incubated with DOX (at a high 30 μg/mL concentration), FeCo/GC, or PBS (Figure 3a and b). However, at a lower dose of free DOX (2 μg/mL), obvious enhancement of DOX toxicity was observed when the cellular incubation was carried out at 43 °C *vs* 37 °C incubation (Figure 3c).

To understand the cell toxicity results, we investigated the effects of hyperthermia on MCF-7 cellular uptake of FeCo/GC−DOX. Cellular uptake of FeCo/GC−DOX at 37 °C *vs* 43 °C was assessed by using MRI. The high relaxivities of FeCo/GC nanocrystals (r_1= 31 and r_2= 185 $mM^{-1}s^{-1}$ at 1.5 T), attributed to the FeCo alloy core, make this material a highly sensitive positive (T_1) and negative (T_2) contrast agent.[19] In a 1 T field, the cells incubated with FeCo/GC−DOX at 43 °C appeared much brighter than either the untreated cells or the cells incubated with FeCo/GC−DOX at 37 °C (Figure 4a). The increase in MRI signal was quantified by region of interest (ROI) measurements of the cell pellets in Figure 4b. The cells incubated at 43 °C had a higher mean intensity than cells incubated at 37 °C or nontreated cells, due to T_1 contrast enhancement by the magnetic nanocrystals. The results indicate higher cellular uptake of FeCo/GC−DOX at 43 °C compared to 37 °C.

Fluorescence and flow cytometry measurements of DOX fluorescence in cells that were incubated with FeCo/GC−DOX at 37 and 43 °C confirmed the MRI results. In Figure 4c, the DOX fluorescence intensity from lysed cells following a 20 min incubation with FeCo/GC−DOX at 43 °C was almost double that of the fluorescence intensity measured from cell lysate following incubation at 37 °C for 20 min. DOX fluorescence from cells measured by flow cytometry confirmed the increased cellular uptake of FeCo/GC−DOX at hyperthermic conditions (Figure 4d). While all cells incubated with FeCo/GC−DOX showed increased fluorescence over MCF-7 cells without FeCo/GC−DOX, the fluorescence of cells incubated at 43 °C for 20 min was 1.9 times greater than that of cells incubated at 37 °C for 20 min. These results confirm the ~two-fold enhanced cellular uptake of FeCo/GC−DOX at 43 *vs* 37 °C. The agreement in MRI and fluorescence results suggests that the hyperthermic incubation enhanced the uptake of the complete FeCo/GC−DOX complex, rather than increasing the uptake of only a single component. In addition, flow cytometry measurements did not show a significant increase in free DOX uptake when incubated at elevated temperatures (see Figure S3, Supporting Information).

It has long been established that endocytosis is an energy-dependent process showing a dependence on temperature and adenosine triphosphate (ATP) levels.[28−30] Cellular endocytosis proceeds at 37 °C, yet is

severely hindered at lower temperatures (*e.g.*, 4 °C).[28,29] Previous studies have indicated clathrin-dependent endocytosis as the mechanism of carbon nanotube uptake into mammalian cells.[30,31] It is expected that FeCo/GC is endocytosed in a similar manner to carbon nanotubes due to the similar graphitic surface and phospholipid coating, with cellular uptake dependent upon temperature, thereby leading to greater uptake of FeCo/GC−DOX conjugates at 43 over 37 °C. Notably, 20 min at 43 °C is well tolerated by the MCF-7 cells, as we observed in this work.

While the photothermally enhanced cellular uptake of FeCo/GC−DOX mostly explains the enhanced cellular toxicity observed herein (Figure 3a), many previous reports suggest enhanced toxicity of DOX at temperatures around 43 °C.[14,18,32,33] To investigate if this was a potential mechanism for enhancement of FeCo/GC−DOX toxicity under hyperthermic conditions, we tested the toxicity of free DOX on cells when incubated for 20 min at 37 or 43 °C. At high free DOX concentrations, *e.g.* 30 μg DOX/mL, the drug is very effective at inhibiting cell growth. At these high doses, cell toxicity appears to be independent of temperature during the 20 min incubation period. This is in good agreement with previous observations that drug doses most effective at normal temperatures do not necessarily demonstrate higher efficacy at elevated temperatures.[16,33] At a much lower dose of 2 μg/mL free DOX, however, there is a significant enhancement of toxicity when the incubation is done at 43 °C, as seen in Figure 3c. This indicates that heating to 43 °C increases the toxicity of DOX when the drug alone is not capable of killing the majority of cells. For cells incubated for 20 min at 37 °C, the lower dose of free DOX (2 μg/mL) more closely resembles the FeCo/GC−DOX incubations in Figure 3a and b, where cell growth is inhibited by less than 30%. At moderately toxic concentrations of either free DOX or FeCo/GC−DOX, exposure of cells to 43 °C for 20 min could enhance the cellular toxicity of DOX delivered *via* FeCo/GC. Therefore, the photothermally enhanced toxicity of FeCo/GC−DOX is likely due to the synergistic effects of increased cellular uptake of FeCo/GC−DOX at 43 °C and an increase in DOX toxicity at elevated temperatures.

The photothermal enhancement of FeCo/GC−DOX toxicity, synergistically improved by drug delivery through increased cellular uptake and enhanced drug toxicity, suggests that photothermally enhanced delivery of DOX *via* highly magnetic FeCo/GC under NIR irradiation could be a powerful technique for cancer therapy and imaging. The NIR laser irradiation conditions used in this work afford selective heat generation only in the presence of FeCo/GC, without which no heating of cells or tissues was observed.

While the use of FeCo/GC−DOX has only been evaluated *in vitro* this system could readily be translated to an *in vivo* treatment method. Previous studies using DOX-loaded single-walled carbon nanotubes (SWNTs) for *in vivo* cancer treatment resulted in higher DOX levels in tumors due to high SWNT accumulation *via* the enhanced permeability and retention effect.[22] In addition, DOX delivery *via* SWNTs reduced systemic drug-related toxicity and resulted in longer survival times of SWNT-DOX treated mice.[22] It is predicted that FeCo/GC−DOX may accumulate in tumors with similar or even higher efficiency than SWNTs due to their ultrasmall size. Uptake of FeCo/GC−DOX could be further increased through the addition of a tumor-targeting ligand on the terminus of the PEG chain. Accumulation of FeCo/GC−DOX in a tumor would enable selective photothermal heating of the tumor region by 808 nm laser irradiation. Photothermally enhanced drug delivery by FeCo/GC and NIR laser irradiation, in combination with enhanced drug efficacy at 43 °C, could lead to a dramatic improvement in chemotherapeutic response *in vivo*. The enhanced susceptibility of malignant cells, over nonmalignant normal cells, to temperatures between 41 and 43 °C could further enhance the efficacy of this treatment while minimizing toxicity to healthy cells.[34] In addition, the reduced toxicity of FeCo/GC−DOX over free DOX at 37 °C could lower the systemic toxicity associated with chemotherapy.[22] Furthermore, MRI contrast enhancement from FeCo/GC could be used as a tool to guide therapy and monitor the tumor response. These features warrant future investigations into the use of FeCo/GC−DOX as an integrated nanoparticle system for combined cancer imaging, drug delivery, and photothermal therapy.

CONCLUSION

In this work we developed an ultrasmall (~4 nm core size) magnetic nanocrystal system for combined drug delivery, imaging, and NIR-induced hyperthermia. In addition to unique supramolecular drug loading and desirable pH sensitive release, we are able to take advantage of the photothermal heating of FeCo/GC to significantly enhance the efficacy of the FeCo/GC−DOX system when heated to 43 °C for 20 min. Investigations into the cause of the enhanced efficacy of FeCo/GC−DOX when combined with 20 min of photothermal therapy revealed a two-fold increase in cellular uptake of FeCo/GC−DOX at 43 °C over 37 °C. This increased cellular uptake, combined with increased DOX toxicity at 43 °C at the relevant dosage, explains the significant enhancement of FeCo/GC−DOX when combined with 808 nm laser irradiation. Laser irradiation did not affect cells incubated with free DOX, FeCo/GC, or with PBS control cells. In addition, exposure of cells to 43 °C for 20 min without drugs present did not significantly affect the cell viability. Photothermally enhanced drug delivery enabled by the

highly integrated FeCo/GC−DOX system could offer a new method of highly effective drug delivery and cancer imaging, while reducing systemic drug-related toxicity.

METHODS

FeCo/GC Synthesis. FeCo/GC nanocrystals were prepared as previously described.[19,20] Briefly, iron nitrate and cobalt nitrate were dissolved in methanol and combined with silica powder to make a growth catalyst. Nanocrystals were formed using methane chemical vapor deposition (CVD) for 5 min at 800 °C. Silica was removed by HF etching, followed by washing with 10% ethanol and finally pure water. Samples were solubilized by sonicating with 1.8 mg/mL phospholipid-branched polyethylene glycol-carboxylate (PL-brPEG) for 1 h, followed by centrifugation at 15 000 rpm for 6 h to remove any aggregates. PL-brPEG was synthesized as previously described.[20]

Drug Loading on FeCo/GC. Prior to drug loading, excess PL-brPEG was removed by washing twice through a 100 kDa centrifuge filter (Millipore). DOX loading was achieved by simple mixing of aqueous DOX solution and ~600 nM FeCo/GC. Under standard loading conditions, the loading was done in 1 × PBS and 1.7 mM DOX, with the pH adjusted to 8.5− 9 using 0.5 M carbonate buffer. For DOX loading tests the DOX concentration was varied from 0.5 to 2 mM during loading, and the pH was adjusted from pH 5−9 using dilute HCl or carbonate buffer. Samples were incubated for ~14 h at room temperature with gentle agitation. After the incubation period, DOX that was not loaded onto the surface of FeCo/GC was removed *via* filtration through a 100 kDa centrifuge filter. Samples were washed with PBS then water a minimum of six times until no DOX was detected in the filtrate. To remove any aggregates, samples were centrifuged for 5 min at 10 000 g.

The concentration of DOX or FeCo/GC was determined by UV−vis using a DOX extinction coefficient of 10 500 M^{-1} cm^{-1} at 490 nm. All UV−vis was done using a Cary 300 spectrophotometer (Varian). The nanocrystal concentration of FeCo/GC was determined by measuring the absorbance at 808 nm, using an extinction coefficient of 3.5 × 10^6 $M^{-1}cm^{-1}$. The extinction coefficient was calculated by relating the graphite absorption at 808 nm to the metal content of a nanocrystal solution and the calculated metal content of a single 4 nm diameter nanocrystal.[19] When both DOX and FeCo/GC were present, the DOX absorbance was extracted by subtracting the background FeCo/GC signal normalized at 808 nm. Concentrations of FeCo/GC−DOX used during experiments are reported as DOX concentration in solution.

DOX Release Tests. FeCo/GC−DOX samples were filtered thoroughly and placed in 3500 MWCO dialysis membranes (Fisher) and placed in PBS at either pH 7.4 or 5.5 after adjusting with HCl. Three separate bags were dialyzed at each condition with aliquots taken at different intervals for determination of DOX loading.

NIR Laser Photothermal Heating. Samples were irradiated using an 808 nm fiber coupled laser (RMPC Lasers). For solution heating, samples containing 450 μM DOX (260 μg DOX/mL) or equivalent FeCo/GC concentration were irradiated with the laser at a power density of 0.3 W/cm^2 for 10 min. The temperature of all samples was monitored using a thermal camera (Mikron Infrared, Oakland, NJ) and periodically confirmed using a thermocouple. The heating curve was determined by measuring the images and plotting the average temperature ± the standard deviation.

Cell Culture and Viability Tests. MCF-7 cells were cultured using Dulbecco's modified eagle medium containing 4.5 g/L D-glucose, 110 mg/L sodium pyruvate, and L-glutamine supplemented with 10% fetal bovine serum and 1% penicillin and streptomycin. Cells were cultured at 37 °C in a humidified atmosphere containing 5% CO_2. For IC_{50} measurements, MCF-7 cells were plated into 96-well plates and allowed to adhere prior to addition of varying concentrations of DOX or FeCo/GC−DOX in PBS. Samples were incubated for 2 days before washing the wells to remove the drugs and replacing the medium. Viability was measured by adding CellTiter 96 (Promega) into the medium. The color change was quantified by measuring the absorbance at 490 nm using a plate reader. Viability is plotted as the fraction of the nontreated control wells.

For laser irradiated and thermally heated cell viability tests, MCF-7 cells were allowed to adhere to a 96-well plate before adding in drug or FeCo/GC samples. Samples were incubated with cells during the 20 min laser irradiation/heating period. During the laser irradiation period, temperatures were closely monitored using a thermal camera and thermoprobe, and the laser power was adjusted to maintain the temperature of FeCo/GC containing wells at ~43 °C. There was little to no nonspecific heating of the DOX or PBS control wells during this laser irradiation. For thermal heating, 96-well plates were heated in a water bath connected to a temperature controller allowing for the temperature to be regulated at either 37 or 43 °C.

Following the 20 min drug incubation, cells were washed three times, replaced with fresh medium, and allowed to grow for 2 days before replacing the medium once more and measuring the viability as discussed above. All samples are plotted as the fraction of nonirradiated/nonheated cells mixed with PBS.

MRI Determination of FeCo/GC−DOX Cell Uptake. For cellular uptake tests, vials of MCF-7 cells were incubated with 100 μM FeCo/GC−DOX for 20 min in a thermally regulated water bath. Following the incubation cells were washed thoroughly and put in fresh vials mounted in an agar phantom. MRI was done using a 1 T small animal scanner (M2, Aspect, Israel) using a steady-state gradient recalled echo sequence (T_r = 9 ms, T_e= 3 ms). Lightening of the cell pellets was indicative of FeCo/GC−DOX uptake and was confirmed by taking ROI measurements of the pellet regions using ImageJ software (NIH). Error bars represent the average of five measurements between two vials incubated at each condition.

Fluorescence Determination of FeCo/GC−DOX Cell Uptake. MCF-7 cells were plated at equal cell densities into 24-well plates and allowed to adhere. After 1 day, cell medium was replaced with Hank's balanced saline solution (HBSS) containing FeCo/GC−DOX at a DOX concentration of 30 μg/mL. Cells were incubated for 20 min in a water bath maintained at either 37 or 43 °C. Following the incubation cells were washed with cold HBSS and then lysed using 0.75% Triton-X 100 in water. DOX was removed from the surface of FeCo/GC by adding acidified isopropanol (0.3 N HCl) and extracting at −20 °C overnight. Equal volumes of extracts and blanks were added to a multiwell plate, and DOX fluorescence was measured using a plate reader (ex. 485 nm, em. 580 nm). Background subtracted DOX signal was plotted in Figure 4c. The error bars represent the standard deviation of four samples at each temperature. Flow cytometry samples were prepared by incubating cells with 575 nM FeCo/GC−DOX or PBS for 20 min at 37 or 43 °C. Cells were washed thoroughly, and measurements were performed on a LSR II flow cytometer. DOX fluorescence from gated, singlet MCF-7 cells was monitored using the phycoerythrin (PE) channel (532 nm excitation, 575/25 nm emission bandpass filter).

Acknowledgment. This work was supported by NIH-1R21CA-133492 and NSF CHE-0639053. We thank the Stanford Small Animal Imaging Facility for the MRI.

Supporting Information Available: DOX fluorescence quenching when loaded on FeCo/GC, cell viability assay of FeCo/GC without DOX, and cellular uptake of DOX under hyperthermic conditions. This material is available free of charge *via* the Internet at http://pubs.acs.org.

REFERENCES AND NOTES

1. Purushotham, S.; Chang, P. E. J.; Rumpel, H.; Kee, I. H. C.; Ng, R. T. H.; Chow, P. K. H.; Tan, C. K.; Ramanujan, R. V. Thermoresponsive Core-Shell Magnetic Nanoparticles for Combined Modalities of Cancer Therapy. *Nanotechnology* **2009,** *20*, 305101.

2. Maeng, J. H.; Lee, D. H.; Jung, K. H.; Bae, Y. H.; Park, I. S.; Jeong, S.; Jeon, Y. S.; Shim, C. K.; Kim, W.; Kim, J.; *et al.* Multifunctional Doxorubicin Loaded Superparamagnetic Iron Oxide Nanoparticles for Chemotherapy and Magnetic Resonance Imaging in Liver Cancer. *Biomaterials* **2010,** *31*, 4995–5006.
3. Park, H.; Yang, J.; Lee, J.; Haam, S.; Choi, I. H.; Yoo, K. H. Multifunctional Nanoparticles for Combined Doxorubicin and Photothermal Treatments. *ACS Nano* **2009,** *3*, 2919–2926.
4. Lee, S. M.; Park, H.; Yoo, K. H. Synergistic Cancer Therapeutic Effects of Locally Delivered Drug and Heat Using Multifunctional Nanoparticles. *Adv. Mater.* **2010,** *22*, 4049–53.
5. Torchilin, V. P. Targeted Pharmaceutical Nanocarriers for Cancer Therapy and Imaging. *AAPS J.* **2007,** *9*, E128–E147.
6. Derfus, A. M.; von Maltzahn, G.; Harris, T. J.; Duza, T.; Vecchio, K. S.; Ruoslahti, E.; Bhatia, S. N. Remotely Triggered Release from Magnetic Nanoparticles. *Adv. Mater.* **2007,** *19*, 3932–3936.
7. Derfus, A. M.; Chen, A. A.; Min, D. H.; Ruoslahti, E.; Bhatia, S. N. Targeted Quantum Dot Conjugates for Sirna Delivery. *Bioconjug. Chem.* **2007,** *18*, 1391–6.
8. Peer, D.; Karp, J. M.; Hong, S.; FarokHzad, O. C.; Margalit, R.; Langer, R. Nanocarriers as an Emerging Platform for Cancer Therapy. *Nat. Nanotechnol.* **2007,** *2*, 751–760.
9. Cheon, J.; Lee, J. H. Synergistically Integrated Nanoparticles as Multimodal Probes for Nanobiotechnology. *Acc. Chem. Res.* **2008,** *41*, 1630–40.
10. Robinson, J. T.; Welsher, K.; Tabakman, S. M.; Sherlock, S. P.; Wang, H.; Luong, R.; Dai, H. High Performance in Vivo Near-IR (>1 μm) Imaging and Photothermal Cancer Therapy with Carbon Nanotubes. *Nano Res.* **2010,** *3*, 779–793.
11. Liu, Z.; Tabakman, S.; Welsher, K.; Dai, H. Carbon Nanotubes in Biology and Medicine: In Vitro and in Vivo Detection, Imaging and Drug Delivery. *Nano Res.* **2009,** *2*, 85–120.
12. Wust, P.; Hildebrandt, B.; Sreenivasa, G.; Rau, B.; Gellermann, J.; Riess, H.; Felix, R.; Schlag, P. M. Hyperthermia in Combined Treatment of Cancer. *Lancet Oncol.* **2002,** *3*, 487–497.
13. Falk, M. H.; Issels, R. D. Hyperthermia in Oncology. *Int. J. Hyperthermia* **2001,** *17*, 1–18.
14. Tang, Y.; McGoron, A. J. Combined Effects of Laser-ICG Photothermotherapy and Doxorubicin Chemotherapy on Ovarian Cancer Cells. *J. Photochem. Photobiol., B* **2009,** *97*, 138–44.
15. Park, J.-H.; von Maltzahn, G.; Xu, M. J.; Fogal, V.; Kotamraju, V. R.; Ruoslahti, E.; Bhatia, S. N.; Sailor, M. J. Cooperative Nanomaterial System to Sensitize, Target, and Treat Tumors. *Proc. Natl. Acad. Sci. U.S.A.* **2010,** *107*, 981–6.
16. Park, J. H.; von Maltzahn, G.; Ong, L. L.; Centrone, A.; Hatton, T. A.; Ruoslahti, E.; Bhatia, S. N.; Sailor, M. J. Cooperative Nanoparticles for Tumor Detection and Photothermally Triggered Drug Delivery. *Adv. Mater.* **2010,** *22*, 880–885.
17. Park, H.; Yang, J.; Seo, S.; Kim, K.; Suh, J.; Kim, D.; Haam, S.; Yoo, K. H. Multifunctional Nanoparticles for Photothermally Controlled Drug Delivery and Magnetic Resonance Imaging Enhancement. *Small* **2008,** *4*, 192–196.
18. Hahn, G. M.; Braun, J.; Harkedar, I. Thermochemotherapy - Synergism between Hyperthermia (42−43 Degrees) and Adriamycin (or Bleomycin) in Mammalian-Cell Inactivation. *Proc. Natl. Acad. Sci. U.S.A.* **1975,** *72*, 937–940.
19. Seo, W. S.; Lee, J. H.; Sun, X. M.; Suzuki, Y.; Mann, D.; Liu, Z.; Terashima, M.; Yang, P. C.; McConnell, M. V.; Nishimura, D. G.; *et al.* Feco/Graphitic-Shell Nanocrystals as Advanced Magnetic-Resonance-Imaging and near-Infrared Agents. *Nat. Mater.* **2006,** *5*, 971–976.
20. Lee, J. H.; Sherlock, S. P.; Terashima, M.; Kosuge, H.; Suzuki, Y.; Goodwin, A.; Robinson, J.; Seo, W. S.; Liu, Z.; Luong, R.; *et al.* High-Contrast in Vivo Visualization of Microvessels Using Novel Feco/Gc Magnetic Nanocrystals. *Magn. Reson. Med.* **2009,** *62*, 1497–1509.
21. Liu, Z.; Sun, X. M.; Nakayama-Ratchford, N.; Dai, H. J. Supramolecular Chemistry on Water-Soluble Carbon Nanotubes for Drug Loading and Delivery. *ACS Nano* **2007,** *1*, 50–56.
22. Liu, Z.; Fan, A. C.; Rakhra, K.; Sherlock, S.; Goodwin, A.; Chen, X. Y.; Yang, Q. W.; Felsher, D. W.; Dai, H. J. Supramolecular Stacking of Doxorubicin on Carbon Nanotubes for in Vivo Cancer Therapy. *Angew. Chem., Int. Ed.* **2009,** *48*, 7668–7672.
23. Sun, X. M.; Liu, Z.; Welsher, K.; Robinson, J. T.; Goodwin, A.; Zaric, S.; Dai, H. Nano-Graphene Oxide for Cellular Imaging and Drug Delivery. *Nano Res.* **2008,** *1*, 203–212.
24. Kataoka, K.; Matsumoto, T.; Yokoyama, M.; Okano, T.; Sakurai, Y.; Fukushima, S.; Okamoto, K.; Kwon, G. S. Doxorubicin-Loaded Poly(Ethylene Glycol)-Poly(Beta-Benzyl-L-Aspartate) Copolymer Micelles: Their Pharmaceutical Characteristics and Biological Significance. *J. Controlled Release* **2000,** *64*, 143–153.
25. Kam, N. W. S.; O'Connell, M.; Wisdom, J. A.; Dai, H. J. Carbon Nanotubes as Multifunctional Biological Transporters and near-Infrared Agents for Selective Cancer Cell Destruction. *Proc. Natl. Acad. Sci. U.S.A.* **2005,** *102*, 11600–11605.
26. Yang, K.; Zhang, S. A.; Zhang, G. X.; Sun, X. M.; Lee, S. T.; Liu, Z. Graphene in Mice: Ultrahigh in Vivo Tumor Uptake and Efficient Photothermal Therapy. *Nano Lett.* **2010,** *10*, 3318–3323.
27. Chance, B. Near-Infrared Images Using Continuous, Phase-Modulated, and Pulsed Light with Quantitation of Blood and Blood Oxygenation. *Ann. N.Y. Acad. Sci.* **1998,** *838*, 29–45.
28. Goldenthal, K. L.; Pastan, I.; Willingham, M. C. Initial Steps in Receptor-Mediated Endocytosis - the Influence of Temperature on the Shape and Distribution of Plasma-Membrane Clathrin-Coated Pits in Cultured Mammalian-Cells. *Exp. Cell Res.* **1984,** *152*, 558–564.
29. Silverstein, S. C.; Steinman, R. M.; Cohn, Z. A. Endocytosis. *Annu. Rev. Biochem.* **1977,** *46*, 669–722.
30. Kam, N. W. S.; Liu, Z. A.; Dai, H. J. Carbon Nanotubes as Intracellular Transporters for Proteins and DNA: An Investigation of the Uptake Mechanism and Pathway. *Angew. Chem., Int. Ed.* **2006,** *45*, 577–581.
31. Kam, N. W. S.; Dai, H. J. Carbon Nanotubes as Intracellular Protein Transporters: Generality and Biological Functionality. *J. Am. Chem. Soc.* **2005,** *127*, 6021–6026.
32. Roti, J. L. R. Cellular Responses to Hyperthermia (40−46 Degrees C): Cell Killing and Molecular Events. *Int. J. Hyperthermia* **2008,** *24*, 3–15.
33. Hildebrandt, B.; Wust, P.; Ahlers, O. Dieing, A.; Sreenivasa, G.; Kerner, T.; Felix, R.; Riess, H., The Cellular and Molecular Basis of Hyperthermia. *Crit. Rev. Oncol. Hematol.* **2002,** *43*, 33–56.
34. Overgaard, J. Effect of Hyperthermia on Malignant Cells in Vivo - Review and a Hypothesis. *Cancer* **1977,** *39*, 2637–2646.